

Analysis and Validations of Modularized Distributed TL-UPQC Systems with Supervisory Remote Management System

Radwa M. Abdalaal, *Student Member, IEEE*, and Carl Ngai Man Ho, *Senior Member, IEEE*

Abstract— Parallel operation of distributed power converters is used to realize high rated power and low current ripples with low rated power devices. It is also being preferred since central compensators fail to identify power quality problems reflected on low voltage levels, especially with the new structure of microgrids. This paper proposes a novel parallel operation between modularized distributed transformerless unified power quality conditioner (TL-UPQC) for low voltage distribution networks. The operation is intended to improve the grid voltage profile while considering the connected modules rated capacity. The proposed methodology is suitable for smart grid applications where multiple renewable energy sources are integrated with the network. An advanced control technique that allows monitoring, wireless communication and coordination between the connected modules is presented. The proposed control methodology allows modularity and operation flexibility. System characterization has been studied to evaluate the influences of communication delays on overall system stability. The system has been evaluated by controller hardware-in-the-loop testing methodology. The power stage is simulated in a real time digital simulator, while the control algorithm is developed in a digital signal processor. Experimental results including random behavior of a photovoltaic system are presented.

Index Terms — D-STATCOM, hardware-in-the-loop, hierarchical control, parallel operation, power quality, UPQC, smart grid, voltage regulation, wireless communication.

I. INTRODUCTION

THE adoption of distributed energy resources (DERs) connected to low voltage (LV) distribution networks has reformed the configuration of the power system dramatically. Therefore, it is essential to reform existing compensation approaches to solve power quality issues as well. A high penetration of photovoltaic (PV) systems installed at residential levels may lead to a sudden voltage rise due to reverse power flow at peak power generation [2]. Partial shading results into a fluctuating power that is reflected on the grid as a fluctuating voltage. Moreover, optimal scheduling and stochastic modeling of electric vehicles charging and discharging scenarios are required in order to avoid voltage drop or overloading on LV distribution networks [3]. A conventional compensation method to improve the grid voltage profile is installing a

centralized distribution static synchronous compensator (D-STATCOM) at medium voltage (MV) distribution networks [4], [5], which requires transformers and switchgears for isolation and protection [6]. This configuration fails to identify local problems elevated at LV distribution network where DER units are connected. It also does not guarantee a stable voltage profile for long distance loads. Compensation units with low power ratings, distributed along LV feeders, would be the right alternative. Distributed compensation units will permit direct interaction between the compensator unit, the utility grid and the load.

Active power filters (APFs) signify a potential solution to maintain high power quality parameters in modern power systems. Unified power quality conditioner (UPQC), which is a combination of series and shunt APFs, is able to suppress power quality issues related to both voltage and current disturbances. The main function of a shunt APF is to improve the power factor and reduce the total harmonic distortion (THD) of the input current. The series converter will provide a stable and a sinusoidal output voltage. Conventional UPQC topologies include a transformer to reduce the voltage stress of the converter [7]. However, transformers are bulky, increase losses and limit the converter's power density. A transformerless UPQC (TL-UPQC) has been proposed in [8]-[11]. While the TL-UPQC topology is able to support loads connected to its output terminal against voltage variations in the network, loads that are connected to the input grid voltage directly are still exposed to these variations. Hence, an additional D-STATCOM is required for voltage regulation at the point of common coupling (PCC) bus [12]. PV systems integrated with UPQCs (PV-UPQC) or shunt APFs (PV-APF) have been proposed in the literature [13], [14]. Thereby besides load reactive power compensation, real power injection into the grid can be realized through the shunt converter. Nevertheless, reactive power injection to regulate the input grid has not been incorporated. The authors in [15] proposed three operating modes that allow the shunt converter to operate in full PV mode, full or partial voltage regulation mode. In this case, rating limitation should be considered in the design process.

Parallel operation of shunt APFs will allow load reactive power and harmonic compensation to be shared by multiple converters. Hence, reduce the current stress and achieve high power application. Centralized and decentralized control techniques have been proposed [16]-[20]. In a decentralized control scheme, controllers operate independently based on local information, where each module treats the rest of

Manuscript received Month xx, 2020; revised Month xx, 2020; accepted Month x, 2020. This is an updated version of conference paper [1]. This work was supported in part by a grant from the Canada Research Chairs, Canada (Sponsor ID: 950-230361).

R.M. Abdalaal, and C.N.M. Ho (Corresponding author) are with RIGA Lab, Department of Electrical & Computer Engineering, University of Manitoba, R3T 5V6, Winnipeg, MB, Canada (e-mail: abdalaal@myumanitoba.ca, carl.ho@umanitoba.ca).

connected modules as part of its load [17], [18]. This concept does not require communication and offers the ability of extending the system capacity with slow dynamic response. Alternatively, a centralized control scheme, referred to as load current distribution or power splitting, is simple to implement and provides system redundancy [19], [20]. Parallel operation has been also introduced in microgrid applications. Droop control is a conventional control method to achieve real and reactive power sharing among distributed generation (DG) units in islanded operation [21], [22]. Even though droop characteristics offer cooperative sharing between multiple modules without relying on communication systems, unequal line impedances and units' power ratings lead to a mismatch and poor reactive power sharing [23]-[26]. Hierarchical control strategies, based on communication techniques, have been proposed to guarantee accurate performance for microgrid operation [25], [26]. It should be noted that parallel operation of DG units in islanded microgrids has been extensively studied. On the other hand, parallel operation of modularized converters to achieve power quality improvement has not been well studied yet. In fact, parallel operation of UPQC systems to provide input grid voltage regulation has not been proposed yet.

The contribution of this paper is to propose a novel control strategy for parallel operation of distributed TL-UPQC systems. The TL-UPQCs will be able to provide input grid voltage regulation through means of grid reactive power compensation as illustrated in Fig. 1. In this paper, not only the TL-UPQC system is able to compensate load reactive power, but it will also incorporate input grid reactive power injection. This is achieved through a coordination scheme between modularized TL-UPQC systems to maintain the PCC voltage at a predefined reference voltage level. Each module represents a distributed compensator and can be modelled by a shunt controlled current source and a series controlled voltage source [11]. Further, the unequal reactance of multiple feeders are considered. Table I highlights a comparison between the proposed technology and existing solutions for grid voltage regulations. The advantages of the proposed distributed TL-UPQCs are,

- Parallel operation of TL-UPQCs modules allowing input grid reactive power sharing strategy to regulate the input voltage.
- Improved redundancy allowing multi-module parallel operation while offering high reliability.
- Plug and play feature that does not require identical TL-UPQC modules.
- Smart grid feature by communicating and exchanging information between the distributed modules and the control center.

II. PROPOSED MODULARIZED DISTRIBUTED TL-UPQC SYSTEMS

The concept of parallel operation of distributed TL-UPQCs is to install modularized small rated TL-UPQCs along LV distribution feeders. This will eliminate the need to install a large capacity D-STATCOM device at the main primary

distribution network. The TL-UPQC systems are to be located adjacent to sensitive non-linear loads in the network. Assuming N distributed TL-UPQC units are connected to the network as depicted in Fig. 1. Each TL-UPQC module is forming a distributed compensator between the network and the load.

A. Individual TL-UPQC module

Fig. 2 illustrates the topology and the structure of the proposed parallel operation of distributed TL-UPQCs for an individual module n in the network, where the parameter's superscript indicates the module's number. The module consists of two voltage source converters that are controlled separately and independently through means of voltage and current controllers. Each module is equipped with a local controller (LC) that collects local measurements. A Wi-Fi module is attached to the LC to allow exchanging information between the system and the control center. The central controller (CC) manages the coordination scheme between the modules wirelessly through internet.

The LC of the TL-UPQC system controls the module's series converter and shunt converter. This paper focuses on the operating principle of the shunt converter to support the PCC voltage v_{PCC} . The capability of the series converter to provide a sinusoidal with constant amplitude output voltage $v_o^{(n)}$ has been analyzed and validated in [8]-[10]. The conventional features of the shunt converter is to compensate load reactive power and mitigate load harmonics. In this paper, the shunt converter can take a role in injecting reactive power into the grid as well. As a result, the system is able to mitigate long and short voltage variations arising at the PCC voltage v_{PCC} . There are three modes of operation: power factor correction (PFC), capacitive and inductive modes. The mode of operation is decided according to the phase angle between the module's PCC current $i_{PCC}^{(n)}$ and the module's point of connection bus voltage $v_B^{(n)}$. The shunt converter of the TL-UPQC system controls the input drawn current to change the mode of operation as follows,

- 1) PFC mode – The PCC current $i_{PCC}^{(n)}$ is controlled to be in phase with $v_B^{(n)}$. Hence, no reactive power injection into the grid is realized.
- 2) Capacitive mode – This mode is activated when the PCC voltage is lower than its reference value. A leading phase angle is created between the $i_{PCC}^{(n)}$ and $v_B^{(n)}$. The whole system has a capacitive reactance characteristic.
- 3) Inductive mode – This mode is activated when the PCC voltage is higher than its reference value. It is contrariwise to the capacitive mode where $i_{PCC}^{(n)}$ is controlled to be lagging and the whole system behaves similar to an inductive reactance.

The PFC mode is the default-operating mode of each module. It offers an independent operation of the CC and relies on local measurements. In this mode, the PCC voltage does not experience voltage variations; hence, no grid reactive power injection is needed. As a result, a sinusoidal and voltage in-phase input current $i_{PCC}^{(n)}(t)$ is drawn from the network bus. The

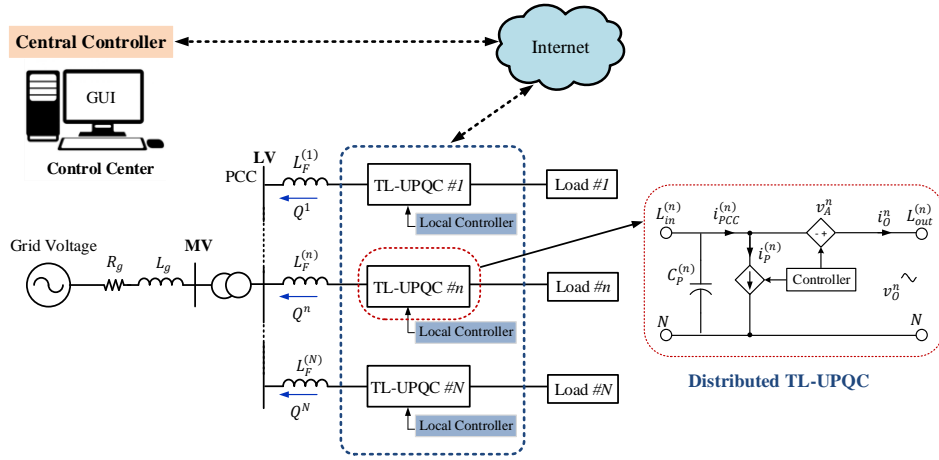


Fig. 1. Proposed modularized distributed TL-UPQC systems architecture.

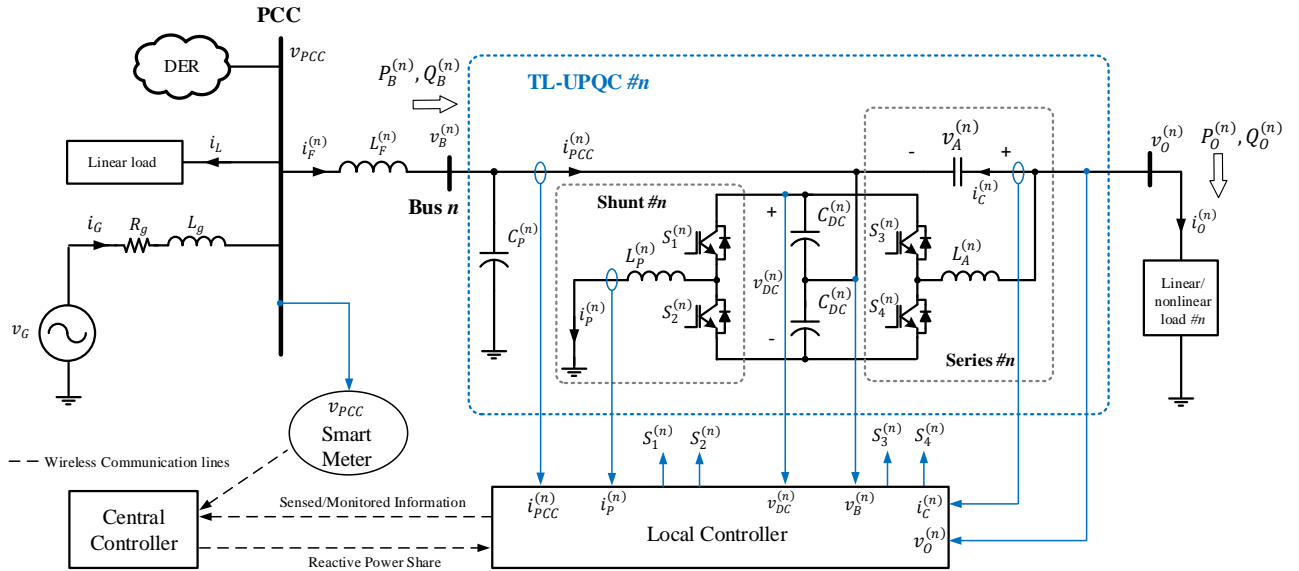


Fig. 2. Topology and structure of an individual TL-UPQC system.

 TABLE I
 COMPARISON BETWEEN VARIOUS TECHNOLOGIES FOR GRID VOLTAGE REGULATION

Technology	Rated Power	Installation	Scalability	Current Quality	Grid Modification
D-STATCOM [5]	> 100 kW	MV	Standalone	Low	Not required
LV D-STATCOM [12]	< 10 kW	LV	Standalone	Improved	Not required
Electric Spring [27]	> 100 kW	LV	Standalone	Low	Required
Proposed solution	1 kW – 1 MW	LV	Scalable	Improved	Not required

module's shunt current $i_p^{(n)}$ contains the opposite components of the harmonic currents that are generated by the load connected to the same feeder and the reactive power requirement for the load to have a resistive load characteristic. Each module has its own synchronization angle developed using phase locked loop (PLL). Consequently, no wireless communication between the distributed TL-UPQC modules is needed.

B. Parallel Operation of TL-UPQC Systems

The coordination between the parallel TL-UPQC modules is

realized via the CC, which is managed by the operator at the distribution substation. The CC monitors the PCC voltage regularly as depicted in Fig. 2. Based on the collected PCC voltage information the CC will initiate the coordination scheme between the TL-UPQC modules to provide input grid voltage regulation. All modules will take part in managing reactive power compensation to support the PCC voltage. The relative strength of the ac system is described by the short circuit ratio (SCR) at the connection point. Low SCR is an indication of a weak grid suffering from high voltage variation. The definition of the SCR is expressed as follows,

$$SCR = \frac{V_{nom}^2}{Z_g S_{nom}} \quad (1)$$

where V_{nom} is the nominal rms voltage of the ac network, Z_g is the grid impedance seen from the PCC point, and S_{nom} is the rated capacity of the DER unit.

To illustrate the theory of operation of the coordination scheme managed by the CC, consider the n^{th} TL-UPQC module in the network. The PCC voltage and the fundamental component of the bus voltage across the n^{th} module can be written as,

$$v_{PCC}(t) = \sqrt{2} V_{PCC} \sin(\omega t) \quad (2)$$

$$v_B^{(n)}(t) = \sqrt{2} V_B^{(n)} \sin(\omega t - \delta_B^{(n)}) \quad (3)$$

where ω is the angular grid frequency, V_{PCC} and $V_B^{(n)}$ are the steady-state rms value of the PCC voltage and the n^{th} module's point of connection bus voltage respectively, while $\delta_B^{(n)}$ is the bus voltage angle corresponding to the PCC voltage.

Different lengths for distribution feeders would lead to line impedance mismatches between the converters and the common bus, causing an unequal voltage drops across the feeder impedances. The real and reactive power transfer between the load bus including the distributed TL-UPQC and the PCC bus are expressed by,

$$P_B^{(n)} = \frac{V_B^{(n)} V_{PCC} \sin \delta_B^{(n)}}{X_F^{(n)}} \quad (4)$$

$$Q_B^{(n)} = \frac{V_B^{(n)} V_{PCC} \cos \delta_B^{(n)} - V_B^{2(n)}}{X_F^{(n)}} \quad (5)$$

where $P_B^{(n)}$ and $Q_B^{(n)}$ are the real and reactive power transfer between the PCC and bus n respectively, while $X_F^{(n)}$ is the equivalent reactance of the n^{th} feeder line.

At the event of a voltage variation in the PCC voltage, the CC establishes a command to request the TL-UPQC to inject/absorb reactive power into/from the grid and support the PCC voltage. A voltage rise in the PCC voltage will require the modules to behave in the inductive mode. Contrarily, a voltage drop in the network will necessitate the operation in the capacitive mode. This is similar to the operation of a D-STATCOM. The difference is that the TL-UPQC is injecting reactive power to the grid besides its respective load reactive power compensation. Therefore, the TL-UPQC rated capacity should be considered. Considering that load bus voltage $v_O^{(n)}$ is being regulated by the series converter, the distributed TL-UPQC systems can perform grid voltage regulation. A phase angle $\theta^{(n)}$ is created between the drawn input current $i_{PCC}^{(n)}(t)$ and the module's point of connection bus voltage $v_B^{(n)}$. The PCC current handled by each module $i_{PCC}^{(n)}(t)$ is expressed by,

$$i_{PCC}^{(n)}(t) = \sqrt{2} I_{PCC}^{(n)} \sin(\omega t - \delta_B^{(n)} \pm \theta^{(n)}) \quad (6)$$

where $I_{PCC}^{(n)}$ is the steady-state drawn PCC current passing through the n^{th} feeder, while $\theta^{(n)}$ is the phase angle of the n^{th} feeder PCC current with respect to the module's point of connection voltage.

The phase angle $\theta^{(n)}$ is governed by the amount of the reactive power that is being injected by the n^{th} module into the grid. It is worth mentioning that the drawn input current $i_{PCC}^{(n)}(t)$ carries the load real power, and the injected reactive power to the grid. Since the CC controller manages the grid reactive power injection, a separate controller that controls the PCC voltage is implemented in the CC. The $i_{PCC}^{(n)}(t)$ is converted to the d-q frame in order to decouple controlling the real and reactive power. The real and the reactive power flow between the TL-UPQC system and the PCC can be accomplished as follows,

$$I_D^{(n)} = I_{PCC}^{(n)} \cos \theta^{(n)} \quad \& \quad P_B^{(n)} = V_B^{(n)} I_D^{(n)} \quad (7)$$

$$I_Q^{(n)} = I_{PCC}^{(n)} \sin \theta^{(n)} \quad \& \quad Q_B^{(n)} = V_B^{(n)} I_Q^{(n)} \quad (8)$$

where $I_D^{(n)}$ and $I_Q^{(n)}$ are the direct and the quadrature component of the PCC feeder current respectively.

Ideally, the TL-UPQC processed real power of the shunt and series converters are balanced in the equilibrium state. The reactive power that is handled by the shunt converter of the TL-UPQC module $Q_P^{(n)}$ can be written as,

$$Q_P^{(n)} = \frac{V_B^{(n)} V_{PCC} \cos \delta_B^{(n)} - V_B^{2(n)}}{X_F^{(n)}} + (V_A^{(n)} - V_O^{(n)}) I_O^{(n)} \sin \phi_O^{(n)} \quad (9)$$

where $V_A^{(n)}$, $V_O^{(n)}$ and $I_O^{(n)}$ are the steady-state series voltage, output voltage and current respectively. $\phi_O^{(n)}$ is the output load phase angle.

It can be observed from (9) that the reactive power share of the module's shunt converter is constrained by the load connected to its output terminal. As mentioned earlier, the module's injected shunt current $i_P^{(n)}$ contains both load reactive power compensation and grid reactive power voltage regulation. Based on the discussed considerations, the control law of the parallel operation of distributed TL-UPQCs is obtained in the next section.

III. CONTROL SCHEME STRUCTURE

The module's series converter controller is implemented in the LC and will remain unchanged to the control law presented in [8]-[10]. The module's series converter is able to boost or reduce its series voltage $v_A^{(n)}$ by applying boundary control with second order switching surface. Adopting boundary control technique enables the system to react to voltage disturbances and return to steady-state operation in two switching cycles, which is adequate for sensitive loads. Accordingly, the voltage across the load $v_O^{(n)}$ is regulated as follows,

$$v_A^{*(n)} = v_O^{*(n)} - v_B^{(n)} \quad (10)$$

where $v_A^*(t)$ and $v_O^*(t)$ are the series voltage reference and the load voltage reference respectively.

The detailed proposed coordination control scheme between the modules' shunt converters is illustrated in Fig. 3. A hierarchical control structure that involves primary and

secondary controllers has been adopted. The primary control represents the LC of each module that collects local measurements. The sensed signals comprising, the module's dc link voltage, the module's inductor current, the module's point of connection voltage and the drawn input current. These signals are sampled and processed by the module's LC. The secondary control, referred to as supervisory controller, includes the CC. The coordination between the modules is achieved via the supervisory controller. A smart meter is placed at the PCC to monitor the PCC voltage v_{PCC} and the injected power by the DER. This information will be sent wirelessly through internet-based communication network to the CC.

There are two control loops in the LC of the module's shunt converter; 1) an outer dc voltage control loop that is responsible of maintaining the module's own dc link voltage and 2) an inner control loop that shapes the module's input current to follow a specified reference current. A second voltage control loop that controls the PCC voltage at a predetermined value is implemented in the CC. This control loop will be referred to as ac voltage control loop. The output of the module's dc voltage control loop specifies the amount of the real power flow to charge up the dc link capacitor and compensates for the converter losses. It also includes the delivered real power to the load connected to the same feeder. The CC is then responsible to command the distributed TL-UPQCs to exchange reactive power between the modules and the grid based on the feedback information transmitted by the smart meter. A centralized coordination scheme has been adopted, in which reactive power compensation is allocated proportionally among all the modules by the supervisory control. Thus, the CC requests each TL-UPQC module to send its measured VA power that is handled by the module's shunt converter $S_p^{(n)}$. The CC will then calculate the proper reactive power share for each module with regard to the module's power rating and its available capacity accordingly. The proportional coefficient $\alpha^{(n)}$ can be found as follows,

$$\alpha^{(n)} = \frac{S_R^{(n)} - S_p^{(n)}}{\sum_{j=1}^N (S_R^{(j)} - S_p^{(j)})} \quad (11)$$

where $S_R^{(n)}$ is the rated capacity of the n^{th} module, while $S_p^{(n)}$ is the module's measured VA.

The total reference reactive power $i_Q^T(t)$ required is generated based on the reference voltage that is assigned by the operator at the CC and the measured PCC voltage. Afterwards, the CC will assign each module to its proportional reactive power share. Internet protocol (IP) address is used to locate individual TL-UPQCs in the network. The amount of the reactive power share of each module that will be transmitted through the network can be expressed as follows,

$$i_Q^{(n)}(t) = \alpha^{(n)} \cdot i_Q^T(t) \quad (12)$$

It can be noted that current reference of the module's input current comprises two components: 1) direct reference current $i_D^{*(n)}(t)$ and 2) quadrature reference current $i_Q^{*(n)}(t)$. The expressions of currents can be expressed as follows,

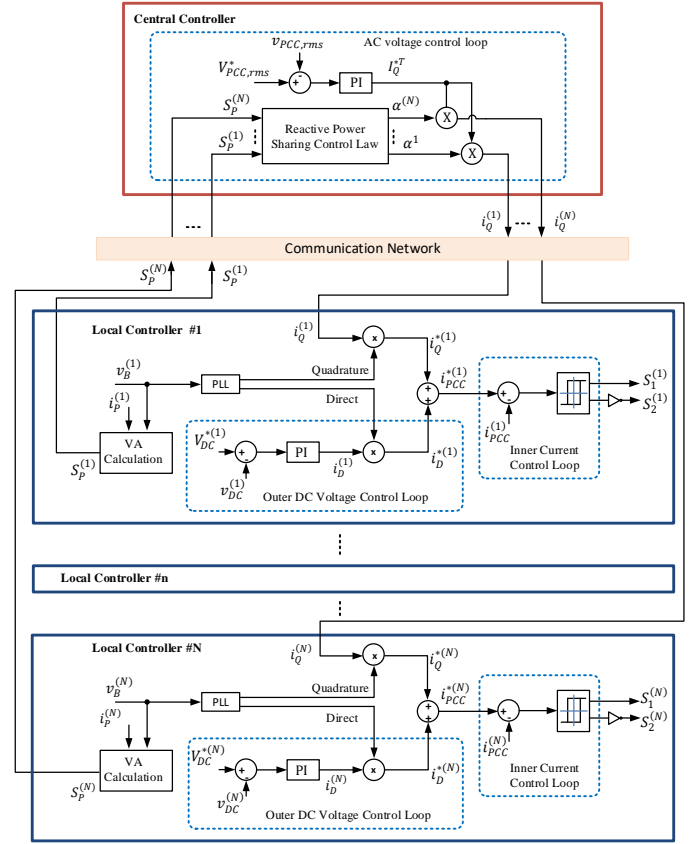


Fig. 3. Control scheme of parallel operation of distributed TL-UPQC systems.

$$i_D^{*(n)}(t) = i_D^{(n)}(t) \sin(\omega t - \delta_B^{(n)}) \quad (13)$$

$$i_Q^{*(n)}(t) = i_Q^{(n)}(t) \cos(\omega t - \delta_B^{(n)}) \quad (14)$$

$$i_{PCC}^{*(n)}(t) = i_D^{*(n)}(t) + i_Q^{*(n)}(t) \quad (15)$$

where $i_{PCC}^{*(n)}(t)$ is the PCC current reference.

Since the injected current follows the module's input voltage PLL, harmonics mitigation is attained. Adopting proportional reactive power sharing control law has the advantage of considering the reactive power and/or the harmonic components of the loads that are required to be compensated by the TL-UPQC system. Non-identical modules can also contribute to the process. This will enhance the plug-n-play feature. In addition, the control law is simple to implement and does not require specific algorithms to estimate the distribution feeders' parameters.

IV. CONTROL SCHEME COORDINATION

To gain insight into the communication delay effect with respect to the system stability, small-signal analysis has been developed. The small-signal control block diagram of one module's LC with its relation to the CC is depicted in Fig. 4. The perturbation in the PCC voltage \tilde{v}_{pcc} is a result of all modules contributing to provide input grid reactive power support. By means of superposition theorem, the perturbation in the PCC voltage can be represented by,

$$\tilde{v}_{pcc}(s) = \sum_{n=1}^N T_{ac}^{(n)}(s) \cdot \tilde{i}_{pcc}^{(n)}(s) \quad (16)$$

Considering one module with its relation to the CC, the transfer functions $T_{dc}^{(n)}(s)$ and $T_{ac}^{(n)}(s)$, which correspond to the dc and ac power stages respectively, can be found deploying state-space analysis as follow,

$$T_{dc}(s) = \frac{\tilde{v}_{dc}^{(n)}(s)}{\tilde{i}_{pcc}^{(n)}(s)} = \frac{2V_B^{(n)}}{s C_{DC}^{(n)} V_{DC}} \quad (17)$$

$$T_{ac}^{(n)}(s) = \frac{\tilde{v}_m^{(n)}(s)}{\tilde{i}_{pcc}^{(n)}(s)} = \frac{L_F^{(n)} [T_G(s) - T_L(s)] s + 1}{T_G(s) - T_L(s) - C_{PS}} \quad (18)$$

$$\text{where, } T_L(s) = \frac{L_g}{L_{eq}} \frac{s + \frac{R_g}{L_g}}{\left(s + \frac{R_L}{L_L + L_F^{(n)}}\right) \left(s + \frac{R_g}{L_g + L_F^{(n)}}\right) - \frac{L_F^{(n)}}{L_{eq}} s^2} \quad (19)$$

$$T_G(s) = \frac{-L_L}{L_{eq}} \frac{s + \frac{R_L}{L_L}}{\left(s + \frac{R_L}{L_L + L_F^{(n)}}\right) \left(s + \frac{R_g}{L_g + L_F^{(n)}}\right) - \frac{L_F^{(n)}}{L_{eq}} s^2} \quad (20)$$

$$L_{eq} = (L_L + L_F^{(n)})(L_g + L_F^{(n)}) \quad (21)$$

R_L and L_L are load parameters connected to the PCC bus, while R_g and L_g are the grid impedance parameters and $L_F^{(n)}$ is the n^{th} feeder impedance parameter. The derivation of (18) is given in the Appendix.

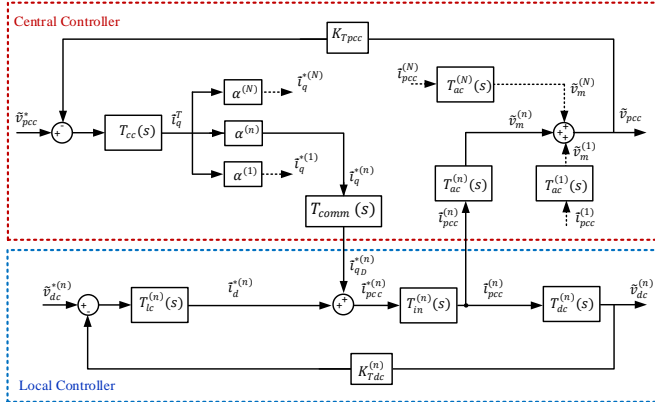


Fig. 4. Small-signal control block diagram of CC and one LC.

The dynamic response of the inner loop is assumed to be very fast with respect to the dc voltage loop. Hence, the transfer function of the inner loop $T_{in}^{(n)}(s)$ can be considered as a constant value throughout the study. The rms value of the output current can be expressed as follows,

$$T_{in}^{(n)}(s) = \frac{K_{PLL}}{\sqrt{2} K_{Ti}} \quad (22)$$

where K_{Ti} is the current sensor gain and K_{PLL} is the PLL gain.

Since the open loop gain of the ac power stage is negative, the CC controller is designed to have a negative gain with the intent to introduce an overall positive gain into the system. In a hierarchal structure, with moving from primary control to secondary control the controller bandwidth should decrease. Therefore, the bandwidth of the CC is designed to be at least 10 times slower than the bandwidth of the LC. In other words, the

proportional K_{Pc} and the integral controller gain K_{Ic} of the CC are chosen such that the controller dynamics are much slower than the controller response of the dc voltage loop. Therefore, the perturbation of the quadrature reference current can be neglected with respect to the LC voltage loop and vice versa. Disregarding the communication delay accompanying the ac voltage control loop, the overall loop gain transfer function of this loop considering one module only can be expressed as,

$$T_{OLq}(s) = -\frac{K_{TPCC} K_{PLL}}{\sqrt{2} K_{Ti}} \left[\frac{K_{Pc} s + K_{Ic}}{s} \times \frac{L_F^{(n)} [T_G(s) - T_L(s)] s + 1}{T_G(s) - T_L(s) - C_{PS}} \right] \quad (23)$$

Fig. 5 shows the Nyquist diagram of the ac voltage loop ignoring the communication delay effect. Given that the system open loop transfer function does not include any pole in the right-half plane and there is zero encirclements around the critical point $(-1, j0)$, the system is stable. Nonetheless, wireless communication usually introduces relatively a large delay in the control loop. The communication delay corresponds to the network latency $T_D(s)$ that depends on the speed of wireless network and the zero order hold (ZOH) $T_{ZOH}(s)$ that represents the delay caused by sampling a continuous time signal. The transfer function of the communication delay can be defined as follows,

$$T_{comm}(s) = T_D(s) \cdot T_{ZOH}(s) = e^{-sT_d} \cdot \frac{(1 - e^{-sT_z})}{sT_z} \quad (24)$$

where T_d is the signal transmission delay and T_z is the ZOH step time delay [28].

Therefore, the overall loop gain transfer function considering the effect of communication delay is expressed as,

$$T'_{OLq}(s) = T_{comm}(s) \cdot T_{OLq}(s) \quad (25)$$

The Nyquist diagrams of the overall loop gain of the ac voltage controller at different time delays are shown in Fig. 6. Even though the diagrams indicate that the system is robust under large delays (1sec), it is worth noticing that the Nyquist plot of the system transfer function T_{OLq} , shown in Fig. 5, did not intersect with the negative real axis indicating an infinite gain margin. However, the transfer function considering the delay T'_{OLq} happens to cross the negative real axis an infinite number of times. Therefore, it is important to evaluate the achievable delay margin for the system to time out. The delay margin corresponds to the maximum delay the system can handle before it becomes unstable.

First analyzing the effect of the ZOH, the ZOH can be further approximated using first order Padé approximation as follows,

$$T_{ZOH}(s) = \frac{(1 - e^{-sT_z})}{sT_z} \approx \frac{s}{s^2 T_z + s} \quad (26)$$

It can be observed that the ZOH acts as a low pass filter. For signals with frequency components that are greater than the Nyquist frequency $\omega_N = \pi/T_z$, aliasing will take place. Typically, an antialiasing filter is added before the sampler to limit the bandwidth of the sampled signals. Moreover, the sampling frequency should be high enough to avoid introducing unwanted phase lags to the designed control system at frequencies lower than the Nyquist frequency.

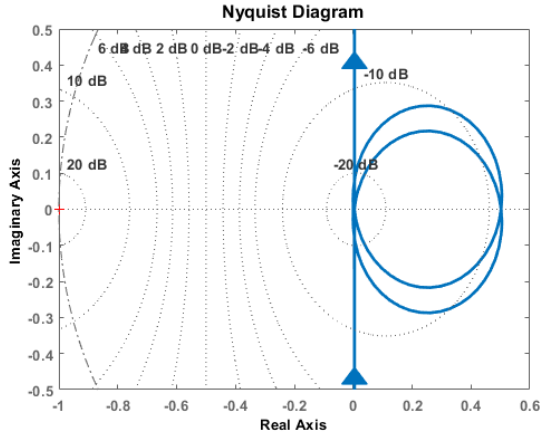


Fig. 5. Nyquist diagram without communication effect $T_{OLq}(s)$.

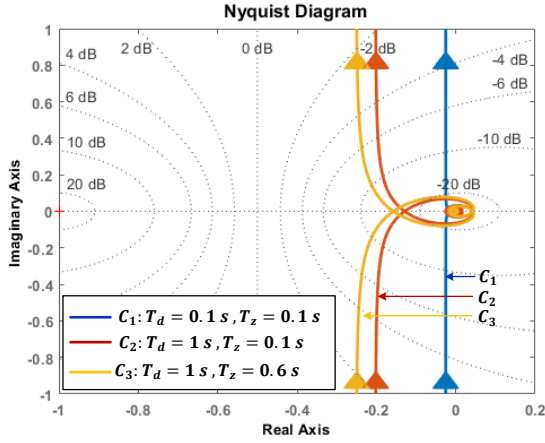


Fig. 6. Nyquist plot under various communication delays $T'_{OLq}(s)$.

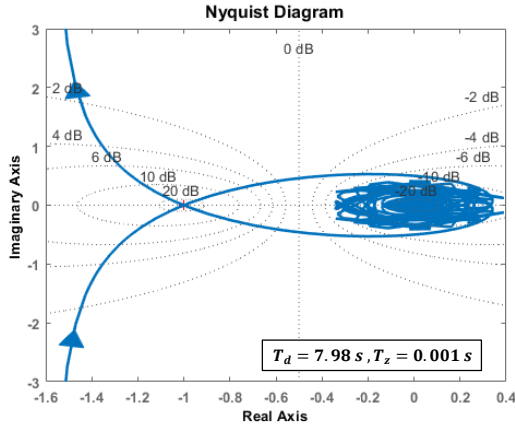


Fig. 7. Marginally stable Nyquist plot of the ac voltage loop.

Table II gives the parameter of the designed control loops including their phase margins. It can be seen that T_z is small enough to nearly have any effect on the designed bandwidth and phase margin (without delay). Unfortunately, this is not the case with the communication signal delay T_d . The reason is that this time delay is not fixed and changes according to the speed of the network. Nevertheless, a maximum achievable delay margin can be set to enable system timeout. The magnitude and phase of the delay transfer function can be found as follows,

$$|T_D(s)| = 1, \angle T_D = -\omega T_d \quad (27)$$

Let PM_i is the phase margin at the frequency ω_i at which,

$$|T_{ZOH}(j\omega_i) \cdot T_{OLq}(j\omega_i)| = 1 \quad (28)$$

Therefore, the effect of the transmission delay signal on the phase margin PM'_i will be as follows,

$$PM'_i = PM_i - \omega_i T_d \quad (29)$$

It can be observed that the main effect of the signal transmission time delay is a reduction of the phase margin. Hence, the maximum delay margin $T_{d,max}$ can be related to the cross over frequency of the system as well as its phase margin as follows,

$$T_{d,max} = PM_i / \omega_i \quad (30)$$

In order for the system to be robust against large delays, it should have a low bandwidth. According to Table II, the delay margin is found to be 7.98 s. Fig. 7 shows that the system is marginally stable at the maximum achievable delay margin where,

$$e^{-j\omega_i T_{d,max}} \cdot T_{ZOH}(j\omega_i) \cdot T_{OLq}(j\omega_i) = -1 \quad (31)$$

If communication is interrupted, an additional ac voltage loop is implemented in the module's LC to regulate the input voltage. In this case, each TL-UPQC system will operate independently from the CC to maintain the module's input voltage ($v_B^{(n)}$) until communication is restored.

TABLE II
COMMUNICATION DELAY EFFECT

Parameters	Value
$T_{OLq}(s)$	$\omega_c = 0.2 \text{ rad/s}, PM_c = 90.2^\circ$
T_z	1 ms
$T_{ZOH}(s) \cdot T_{OLq}(s)$	$\omega_i = 0.2 \text{ rad/s}, PM_i = 90.2^\circ$
$T_D(s) \cdot T_{ZOH}(s) \cdot T_{OLq}(s)$	$T_{d,max} = 7.98 \text{ s}$

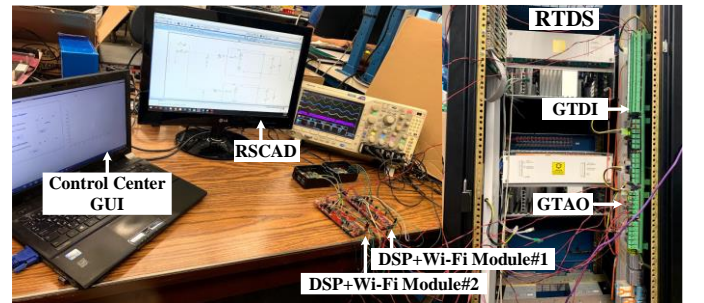


Fig. 8. Controller hardware-in-the-loop (CHIL) testbed.

V. SYSTEM IMPLEMENTATION AND EXPERIMENTAL VERIFICATION

To validate the proposed methodology, a controller hardware-in-the-loop (CHIL) testing methodology has been implemented as shown in Fig. 8. Fig. 9 describes the detailed system implementation structure. The test has been performed on two identical TL-UPQCs with shunt rated capacity each of 2 kVA. The grid network and the TL-UPQC modules are developed and simulated in real time digital simulator (RTDS).

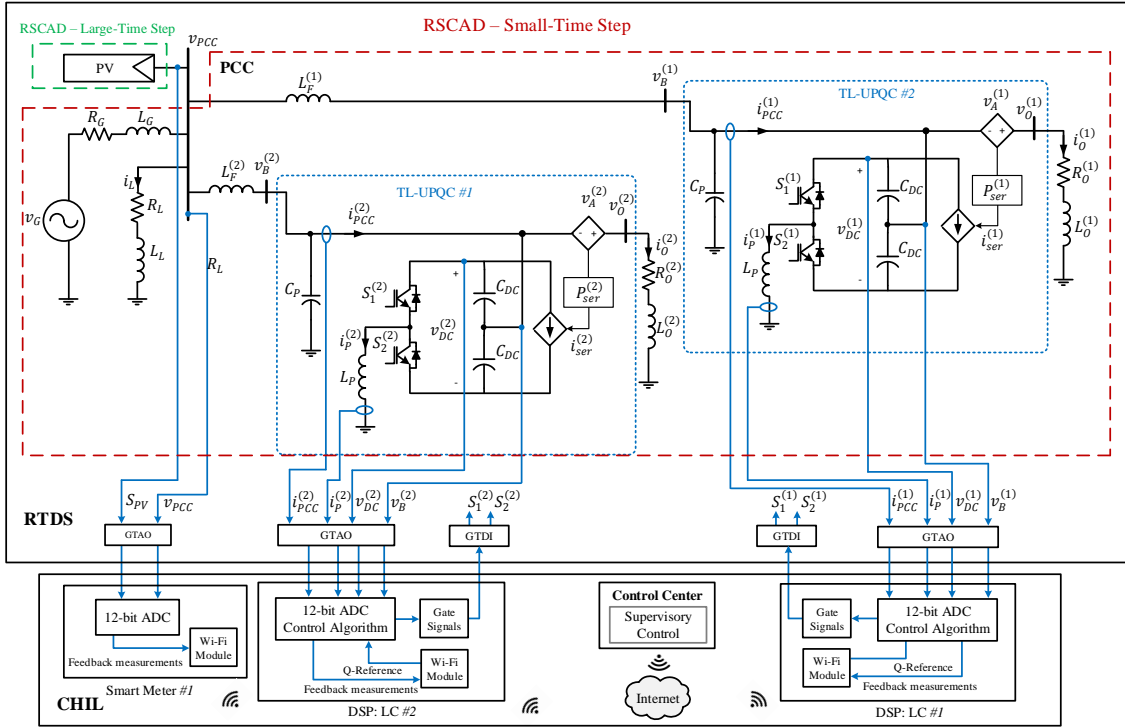


Fig. 9. Block diagram of system implementation using CHIL with RTDS.

RSCAD simulator program has been used for interface with RTDS. The series converter has been modeled as a voltage controlled voltage source that regulates the voltage across the output load as depicted in the figure [11]. While the parallel operation of the shunt converters is the interest of this paper, it is important to include the influence of the series converter on the overall system performance. Therefore, a controlled current source connected to the dc link is modeled inside RTDS, which represents the power needed by the shunt converter to support the series converter. A current source has been connected to the PCC to emulate the behavior of a photovoltaic (PV) system. The PV injected power to the network is intended to create voltage variations in the network. Both the grid and the TL-UPQC modules have been simulated using the small-time step library at $2.2 \mu s$, whereas the PV system, which is modeled as a current source, has been simulated in the large time step at $50 \mu s$. Different loads are connected at the output of TL-UPQCs. The LC has been implemented using a digital signal processor (DSP) F28377S with 12 bit analogue to digital converter (ADC) resolution. The sensed signals to the controller are sent using giga-transceiver analogue output (GTAO) card. The digital interface, giga-transceiver digital input (GTDI) card, provides the gate pulses decided by the DSP to the converters modeled inside RTDS. The CC has been implemented in MATLAB software from which a graphical user interface (GUI) has been developed. Serial peripheral interface (SPI) has been deployed to exchange data between each DSP and its Wi-Fi module.

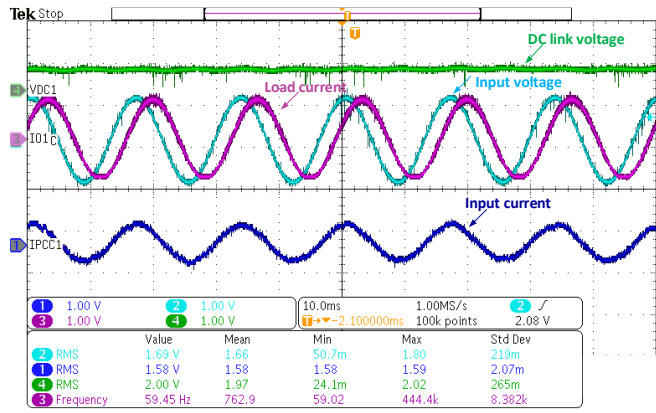
A. Validation of an individual TL-UPQC module

First, the operation of an individual TL-UPQC system will be validated under the CHIL test. The results are compared with the experimental results presented in [9]. The module's LC

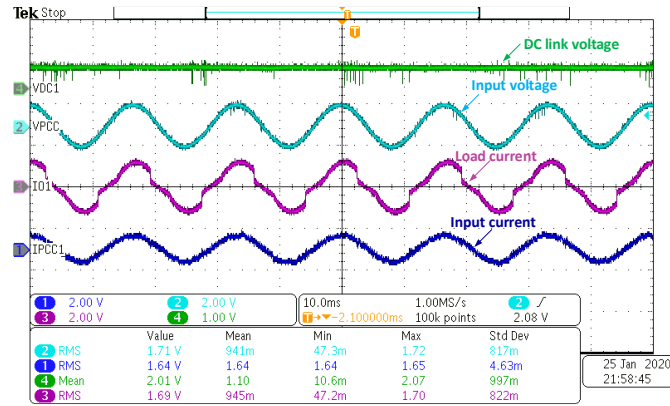
operates independently from the supervisory control in the PFC mode. In this mode, no input grid reactive power compensation is required from the system (i.e. $i_Q^{(1)} = 0$). The results are monitored in an oscilloscope. Note that, the GTAO card includes a 16-bit digital to analogue converter (DAC) and provides an output analogue signal with $\pm 10 V$ output range. Nevertheless, the input signals to the DSP are scaled down within a range of 0-3V. Fig. 10 (a) shows the PFC mode experimental results for a linear load connected to the TL-UPQC output voltage. The results indicate that the shunt converter is able to compensate load reactive power as highlighted in Table III. The results shown in Fig. 10 (b) and (c) corroborate the ability of the system to mitigate harmonics for various nonlinear loads. The load in Fig. 10 (b) comprises a controlled rectifier bridge circuit with a resistive and an inductive load, while the load in Fig. 10 (c) comprises a lighting network composed of LED lamps. Both loads are to be connected to the system output terminals. Power quality measurements of the load current and of the input drawn current in the PFC mode are given in Table III. The results endorse the performance of an individual TL-UPQC to achieve a sinusoidal input current with a total harmonic decision THD_i below 5%.

TABLE III
MEASURED POWER ANALYSIS PARAMETERS FOR VARIOUS NONLINEAR LOADS

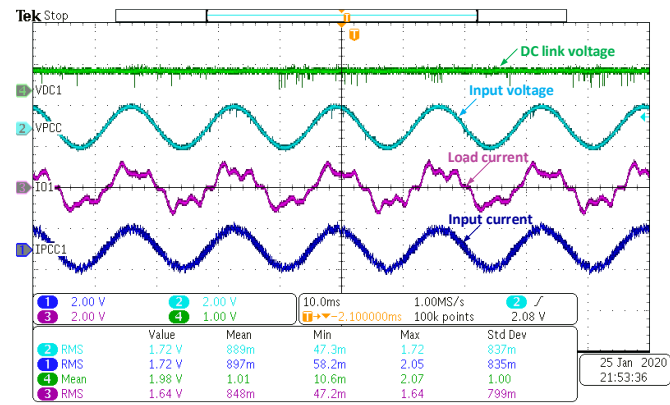
Load under test	Load current	Input current
Case (a)	$PF = 0.55$	$PF = 0.973$
Case (b)	$THD_i = 15.69\%$	$THD_i = 4.34\%$
Case (b)	$THD_i = 32.27\%$	$THD_i = 4.65\%$



(a)



(b)



(c)

Fig. 10. Steady-state waveforms for PFC mode (a) linear (b) nonlinear load-rectifier bridge circuit (c) nonlinear load – LED lamps.

B. Validation of Coordinated Parallel-Operated TL-UPQCs

A case study to validate the proposed coordinated parallel operation of two TL-UPQC modules to provide input grid voltage regulation has been conducted. The PV system rating is 8 kW with an SCR of 0.92. The parameters of the system under study have been specified in Table IV. Fig. 11 shows the GUI that allows the operator to define an ac voltage reference and start the reactive power support operation based on the number of available TL-UPQC modules in the network. The GUI also includes real time data logging and monitoring for the available generated PV power and the PCC voltage measurements. In this test, the PCC voltage is to be regulated at 120V rms. The results

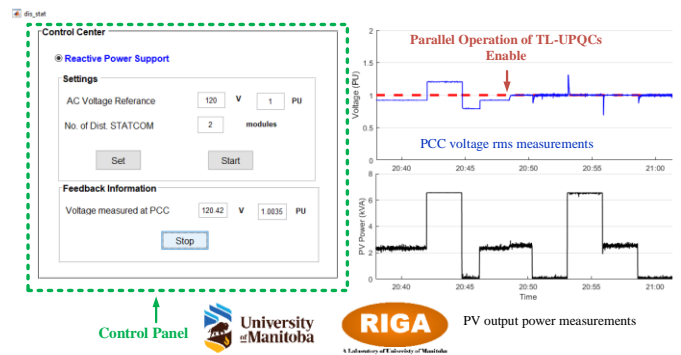
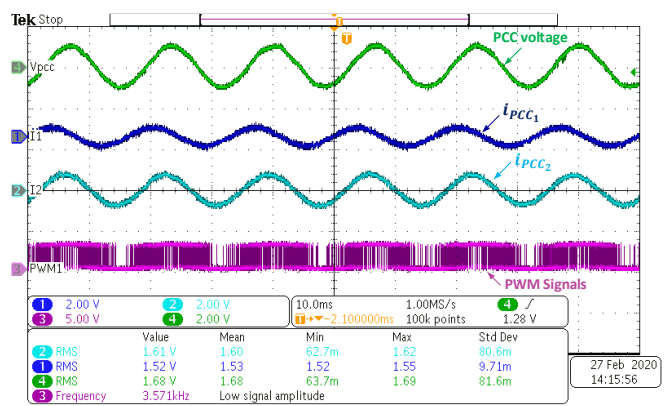
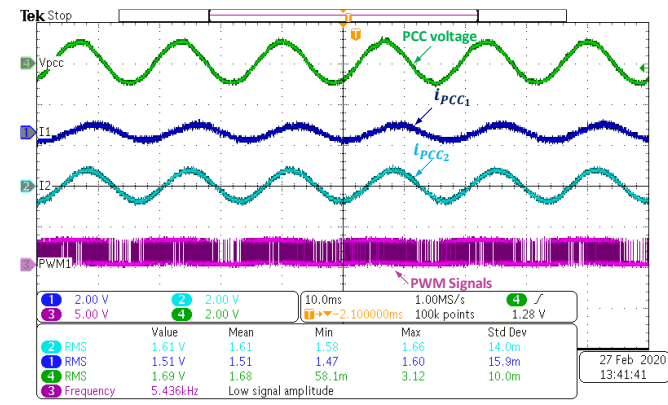


Fig. 11. GUI - control center panel with measured results.



(a)



(b)

Fig. 12. Steady-state waveforms for (a) capacitive mode (b) inductive mode.

shown in Fig. 11 imply that the PCC voltage is fluctuating between 0.8 and 1.2 pu voltage before enabling the parallel operation of the distributed TL-UPQCs. These voltage fluctuations are happening due to the random behavior of the PV injected power as the figure indicates. Nevertheless, the PCC voltage has been maintained at 1 pu after activating the reactive power support of the connected modules. The steady-state waveforms in Fig. 12 (a) show the operation of both modules to support an under voltage at the PCC. In this case, both module are operating in the capacitive mode. It can be seen that both currents are leading the PCC voltage under this mode of operation to boost the PCC voltage. Fig. 12 (b) shows the steady-state waveforms for an over voltage where the modules are operating in the inductive mode. In other words, the injected

TABLE IV
SYSTEM SPECIFICATIONS

Parameters	Value
PCC voltage	120 V
Grid frequency	60 Hz
No. of connected modules N	2
Module's dc link Voltage	400 V
C_{DC}, C_p, L_p	1500 μ F, 47 μ F, 10 mH
R_g, L_g, R_L, L_L	0.5 Ω , 5 mH, 10 Ω , 10 mH
$L_F^{(1)}, L_F^{(2)}$	1 mH, 2 mH
$R_O^{(1)}, L_O^{(1)}, R_O^{(2)}, L_O^{(2)}$	100 Ω , 80 mH, 10 Ω , 20 mH
Dc voltage control loop	$K_{PI} = 0.5, K_{IL} = 0.5$
Ac voltage control loop	$K_{PC} = 0.01, K_{IC} = 0.8$

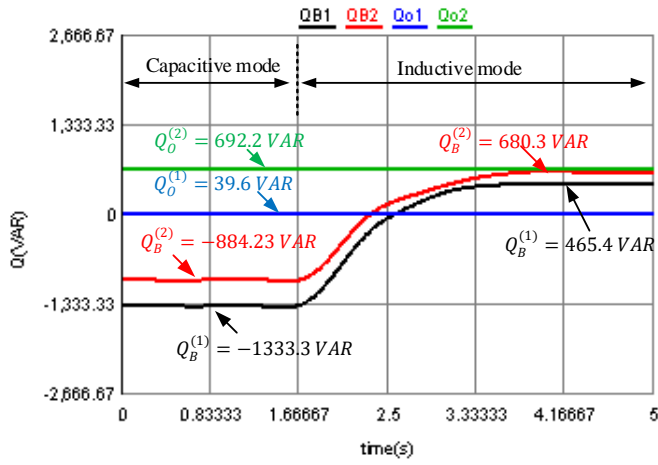


Fig. 13. Reactive power share of each module with the coordination scheme.

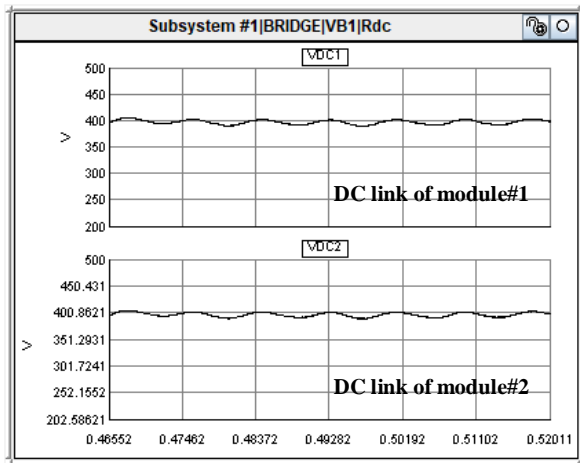
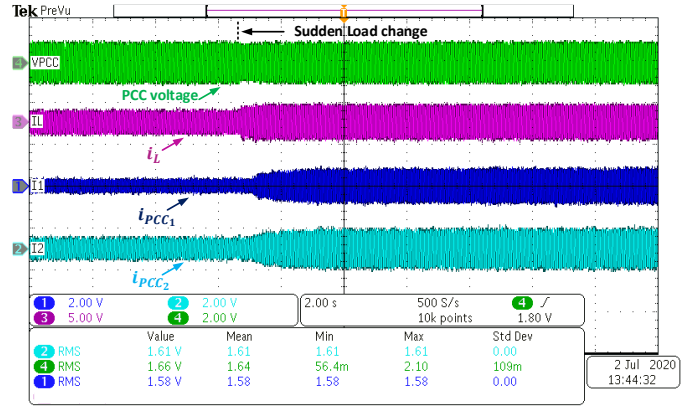
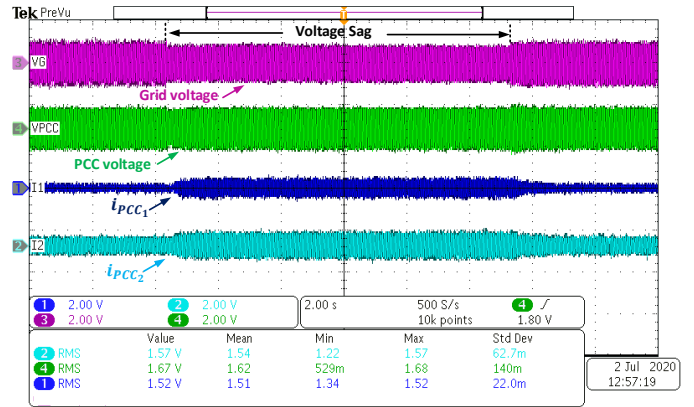


Fig. 14. DC link measurements as captured in RSCAD.

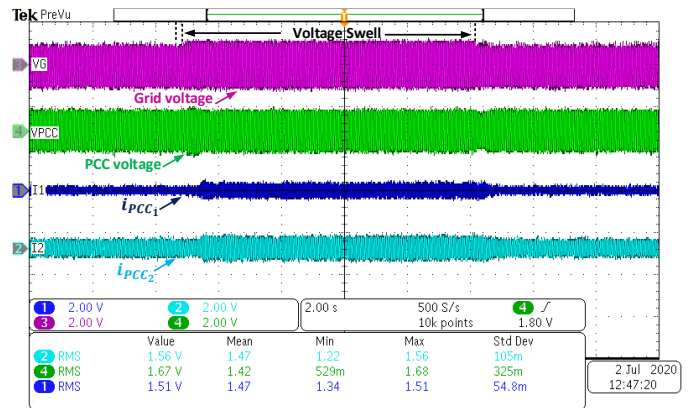
currents by the TL-UPQCs are lagging. In order to support the proposed coordination control scheme results, Fig. 13 shows the input grid reactive power share of each module in both modes ($Q_B^{(1)}, Q_B^{(2)}$) as measured in RSCAD runtime window. In the capacitive mode, the contribution of the first module to



(a)



(b)



(c)

Fig. 15. System waveforms for (a) load change at the PCC bus ($Z_L = 10.7\Omega - 7\Omega$) (b) voltage sag of -10% (c) voltage swell of +10%.

support the grid is larger with 60% share of the total reactive power needed (e.g. $\alpha_1 = 0.6$ and $\alpha_2 = 0.4$). This is expected since the load reactive power compensation required by the second module $Q_o^{(2)}$ is larger the first module $Q_o^{(1)}$. Hence, the second module is already contributing with a larger reactive power portion to its load, which is the module's highest priority. The operation is contradictory in the inductive mode. Both modules' dc link voltages have been maintained at 400V as captured in RSCAD runtime environment in Fig. 14. While the modules are operating in the capacitive mode, a sudden load step up on the PCC (R_L, L_L) has been enabled as shown Fig. 15

(a). This causes an additional voltage drop across the grid impedance and the PCC voltage level. The CC will react accordingly and request the modules to increase their reactive power injection into the grid and hence maintain the PCC voltage level at 120V rms. Since each module is always tracking its PLL, the THD of the input current remains low of 4.7%.

Another test has been conducted to validate the ability of the proposed parallel operation of distributed TL-UPQCs to support loads connected to the PCC voltage under various voltage disturbances. To emulate short duration voltage variations across the PCC bus, the grid voltage v_G has been programmed to vary causing a voltage sag of 108V rms as depicted in Fig. 15 (b). A regulated PCC voltage can be observed regardless of the voltage sag in the network. Similarly, a voltage swell of 132V rms has been applied as indicated Fig. 15 (c). Both modules are able to adjust their reactive power share in response to the change of the PCC voltage level.

C. Communication Failure or Module Failure

The test described in Fig. 13 has been repeated at the event of a communication failure. In this case, there is no coordination between the two modules since the CC is down. The modules will rely on the primary controller information, in other words the module's LC, to restore the modules' point of connection voltages $v_B^{(1)}$ and $v_B^{(2)}$. Fig. 16 presents the reactive power share of each module without the coordination scheme as captured in RSCAD runtime. The voltage waveforms shown in Fig. 17 indicate that the injected reactive powers was sufficient to support the modules' input voltages $v_B^{(1)}$ and $v_B^{(2)}$. Nevertheless, the PCC voltage was not fully restored to 1 pu. Moreover, the systems failed to identify an over voltage at the PCC bus and continue to operate in the capacitive mode. This is due to the voltage drop across the feeders' reactance and the loss of systems coordination.

In the following test, the system's response during a fault in one of the TL-UPQC modules is investigated. Fig. 18, Fig. 19 and Fig. 20 show the results of the reactive power share of each module and system waveforms after the occurrence of a fault in module number 2. The results demonstrate that module number 1 increased its reactive power share according to its available capacity to compensate for the second module's reactive power share loss. While the second module will be out of service with zero shunt converter reactive power injection. Therefore, the reactive power exchange between the second feeder and the PCC bus is the same as the load reactive power consumption. It is worth mentioning that since the reactive power injection is limited by the modules' rated power, the PCC voltage was raised back to only 0.93 pu. Overall system reliability can be increased by increasing the number of the connected parallel-operated TL-UPQC modules.

VI. CONCLUSION

The paper proposed a novel coordinated operation of distributed TL-UPQCs connected to LV feeders. Proportional reactive power sharing technique to support the input grid

voltage based on the unit capacity was presented. A remote management system that represents a centralized supervisory control was proposed. The control commands are sent from the central controller to the local controllers, with no interaction between individual modules. This allow independent operation of the modules if no voltage regulation is necessary or communication is interrupted. A GUI was developed to perform as a supervisory management system in the control center. The communication delay between the central controller and the local controller was considered in the control design criteria. Analysis to estimate the maximum achievable delay margin before the system becomes unstable was developed and validated using Nyquist diagram. The experiment test was conducted in real time simulator with the power stage in RTDS, while controllers are implemented in DSP. The results verified the ability of the TL-UPQC modules to provide grid voltage stability. The coordinated scheme indicated that the PCC voltage profile was improved and maintained at 1 pu. All modules supported the PCC voltage against under/over voltage and compensated for voltage sags/swells. This was achieved in addition to the conventional features of the TL-UPQC system.

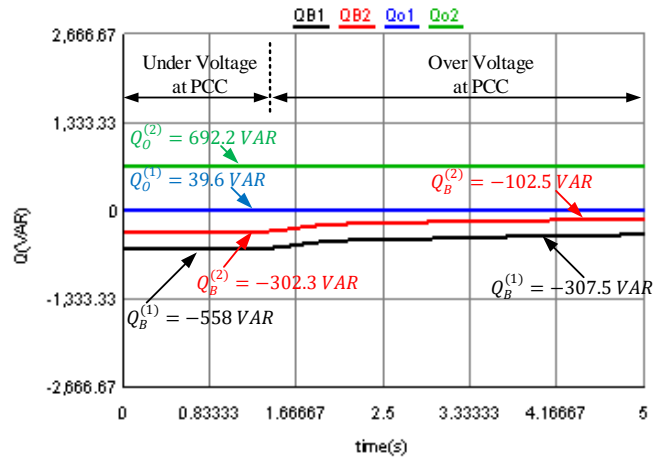


Fig. 16. Reactive power share of each module without the coordination scheme.

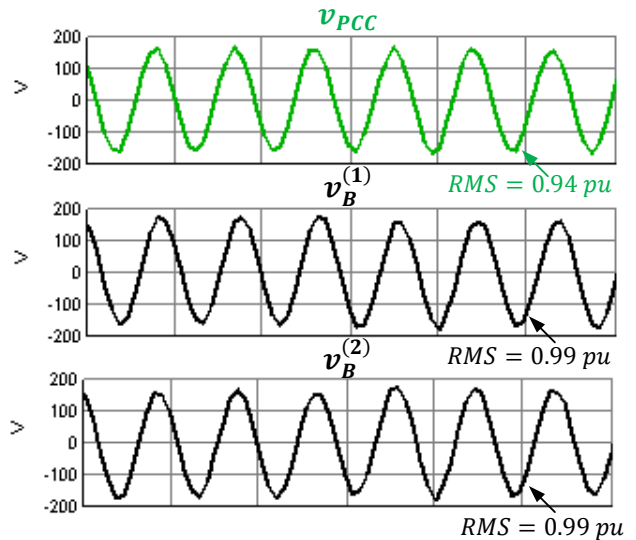


Fig. 17. Voltage waveforms as captured in RSCAD.

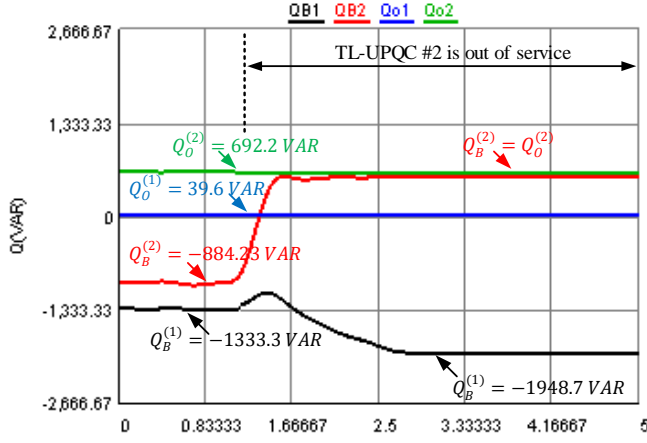


Fig. 18. Reactive power share of each module after a fault in TL-UPQC #2.

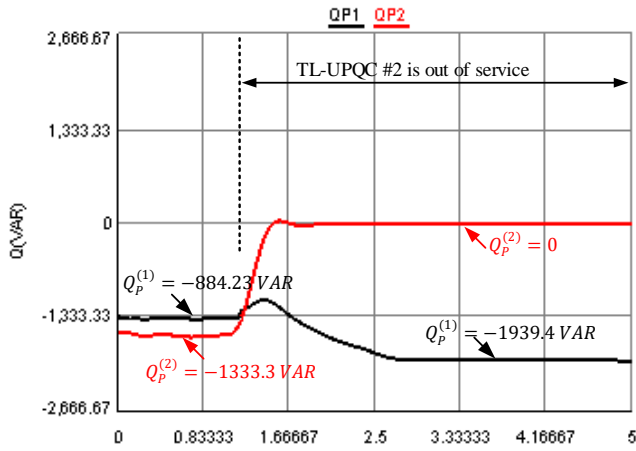


Fig. 19. Shunt converter reactive power share after a fault in TL-UPQC #2.

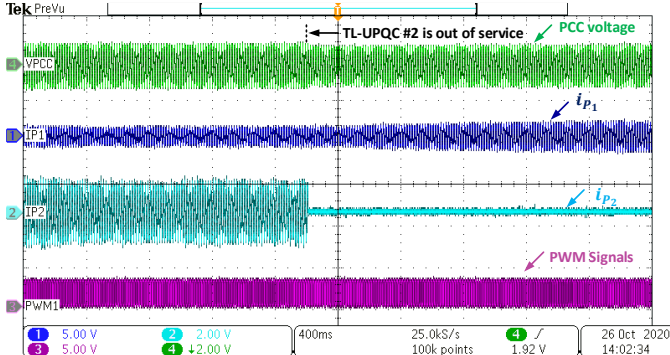


Fig. 20. System waveforms after a fault in TL-UPQC #2.

The experimental results were in good agreements with the theoretical concept and indicated the validation of the coordinated scheme to share grid reactive power injection between modules proportionally.

APPENDIX

Derivation of (18)

The state-space matrices of the distributed TL-UPQC system including the feeder reactance can be found applying superposition for module n . The new set of state-space

equations are described as follows,

$$\begin{bmatrix} 1 & 0 & 0 & 0 & 0 \\ 0 & 1 & 0 & 0 & 0 \\ 0 & 0 & 1 & 0 & 0 \\ 0 & 0 & 0 & (L_L + L_F^{(n)}) & -L_F^{(n)} \\ 0 & 0 & 0 & -L_F^{(n)} & (L_g + L_F^{(n)}) \end{bmatrix} x(t) = \begin{bmatrix} 0 & -\frac{1}{C_P} & 0 & -\frac{1}{C_P} & \frac{1}{C_P} \\ \frac{1}{L_P} & 0 & \frac{1-2q_1(t)}{2L_P} & 0 & 0 \\ 0 & \frac{2q_1(t)-1}{C_{DC}} & 0 & 0 & 0 \\ 1 & 0 & 0 & -R_L & 0 \\ -1 & 0 & 0 & 0 & R_g \end{bmatrix} x(t) + \begin{bmatrix} 0 \\ 0 \\ 0 \\ 0 \\ 1 \end{bmatrix} u(t) \quad (\text{A. 1})$$

and,

$$y(t) = \begin{bmatrix} 1 & 0 & 0 & 0 & 0 \\ 0 & 0 & 1 & 0 & 0 \end{bmatrix} x(t) \quad (\text{A. 2})$$

where,

$$x(t) = \begin{bmatrix} v_B^{(n)}(t) \\ i_{PCC}^{(n)}(t) \\ v_{DC}^{(n)}(t) \\ i_L(t) \\ i_G(t) \end{bmatrix}, u(t) = v_G(t), y(t) = \begin{bmatrix} v_B^{(n)}(t) \\ v_{DC}^{(n)}(t) \end{bmatrix} \quad (\text{A. 3})$$

$$q_1(t) = \begin{cases} 1 & S_1 \text{ off}, S_2 \text{ on} \\ 0 & S_1 \text{ on}, S_2 \text{ off} \end{cases} \quad (\text{A. 4})$$

Small ac perturbations are introduced to the stat-space variables as follows, $v_B^{(n)} = V_B^{(n)} + \tilde{v}_b^{(n)}$, $i_{PCC}^{(n)} = I_{PCC}^{(n)} + \tilde{i}_{pcc}^{(n)}$, $v_{DC}^{(n)} = V_{DC}^{(n)} + \tilde{v}_{dc}^{(n)}$, $i_L = I_L + \tilde{i}_L$ and $i_G = I_G + \tilde{i}_G$. The small-signal equations can be obtained by neglecting the steady-state terms and transferred into the Laplace domain, from which the following can be derived,

$$\frac{\tilde{i}_g(s)}{\tilde{v}_b^{(n)}(s)} = T_G(s) = \frac{-L_L}{L_{eq}} \frac{s + \frac{R_L}{L_L}}{\left(s + \frac{R_L}{L_L + L_F^{(n)}}\right) \left(s + \frac{R_g}{L_g + L_F^{(n)}}\right) - \frac{L_F^{(n)2}}{L_{eq}}} s^2 \quad (\text{A. 5})$$

$$\frac{\tilde{i}_l(s)}{\tilde{v}_b^{(n)}(s)} = T_L(s) = \frac{L_g}{L_{eq}} \frac{s + \frac{R_g}{L_g}}{\left(s + \frac{R_L}{L_L + L_F^{(n)}}\right) \left(s + \frac{R_g}{L_g + L_F^{(n)}}\right) - \frac{L_F^{(n)2}}{L_{eq}}} s^2 \quad (\text{A. 6})$$

where,

$$L_{eq} = (L_L + L_F^{(n)})(L_g + L_F^{(n)}) \quad (\text{A. 7})$$

The perturbation in the PCC voltage \tilde{v}_{pcc} due to reactive power injection of one module will be referred to as $\tilde{v}_m^{(n)}$ where,

$$\tilde{v}_{pcc} = \sum_{n=1}^N \tilde{v}_m^{(n)} \quad (\text{A. 8})$$

And $\tilde{v}_m^{(n)}$ can be expressed as follows,

$$\tilde{v}_m^{(n)} = L_F^{(n)} s (\tilde{i}_g(s) - \tilde{i}_l(s)) + \tilde{v}_b^{(n)}(s) \quad (\text{A. 9})$$

Substituting (A.5) and (A.6) into (A.9), the following can be obtained,

$$\frac{\tilde{v}_m^{(n)}(s)}{\tilde{v}_b^{(n)}(s)} = L_F^{(n)} [T_G(s) - T_L(s)]s + 1 \quad (\text{A. 10})$$

In addition, the relation between the perturbation of the module's point of connection voltage $\tilde{v}_b^{(n)}$ due to the module's injected current $\tilde{i}_{pcc}^{(n)}$ can be expressed as follows,

$$\tilde{v}_b^{(n)} = \frac{1}{C_{PS}} (\tilde{i}_g(s) - \tilde{i}_l(s) - \tilde{i}_{pcc}^{(n)}) \quad (\text{A. 11})$$

$$\frac{\tilde{i}_{pcc}^{(n)}(s)}{\tilde{v}_b^{(n)}(s)} = T_G(s) - T_L(s) - C_{PS} \quad (\text{A. 12})$$

From (A.10) and (A.12), expression (18) can be found.

REFERENCES

- [1] R. Abdalaal and C. Ho, "A Supervisory Remote Management System for Parallel Operation of Modularized D-STATCOM," in *Proc. IEEE Appl. Power Electron. Conf. (APEC)*, 2020.
- [2] M. J. E. Alam, K. M. Muttaqi and D. Sutanto, "An Approach for Online Assessment of Rooftop Solar PV Impacts on Low-Voltage Distribution Networks," *IEEE Trans. Sustainable Energy*, vol. 5, no. 2, pp. 663-672, April 2014.
- [3] R. Leou, C. Su and C. Lu, "Stochastic Analyses of Electric Vehicle Charging Impacts on Distribution Network," *IEEE Trans. Power Syst.*, vol. 29, no. 3, pp. 1055-1063, May 2014.
- [4] T. Lee, S. Hu and Y. Chan, "D-STATCOM With Positive-Sequence Admittance and Negative-Sequence Conductance to Mitigate Voltage Fluctuations in High-Level Penetration of Distributed-Generation Systems," *IEEE Trans. Ind. Electron.*, vol. 60, no. 4, pp. 1417-1428, Apr. 2013.
- [5] A. Khoshooei, J. S. Moghani, I. Candela and P. Rodriguez, "Control of D-STATCOM During Unbalanced Grid Faults Based on DC Voltage Oscillations and Peak Current Limitations," *IEEE Trans. Ind. Appl.*, vol. 54, no. 2, pp. 1680-1690, Mar.-Apr. 2018.
- [6] A. Moreno, *Power Quality: Mitigation Technologies in a Distributed Environment*, London, Springer London, 2007.
- [7] V. Khadkikar, "Enhancing electric power quality using UPQC: A comprehensive overview," *IEEE Trans. Power Electron.*, vol. 27, no. 5, pp. 2284-2297, May 2012.
- [8] N. Ho, R. Abdalaal, and H. Chung, "Transformerless Single-Phase Unified Power Quality Conditioner (UPQC) for Large Scale LED Lighting Networks, US Patent Application, US20190182917A1, 13/06/2019.
- [9] R. M. Abdalaal and C. N. M. Ho, "Transformerless single-phase UPQC for large scale LED lighting networks," in *Proc. IECON Ann. Conf. IEEE Ind. Electron. Soc.*, 2017, pp. 1629-1634.
- [10] V. S. Cheung, R. S. Yeung, H. S. Chung, A. W. Lo and W. Wu, "A Transformer-Less Unified Power Quality Conditioner with Fast Dynamic Control," *IEEE Trans. Power Electron.*, vol. 33, no. 5, pp. 3926-3937, May 2018.
- [11] R. M. Abdalaal, C. N. M. Ho, C. K. Leung and H. S. Chung, "A Remotely Central Dimming System for a Large-Scale LED Lighting Network Providing High Quality Voltage and Current," *IEEE Trans. Ind. Appl.* vol. 55, no. 5, pp. 5455-5465, Sept.-Oct. 2019.
- [12] R. T. Hock, Y. R. de Novaes and A. L. Batschauer, "A Voltage Regulator for Power Quality Improvement in Low-Voltage Distribution Grids," *IEEE Trans. Power Electron.*, vol. 33, no. 3, pp. 2050-2060, Mar. 2018.
- [13] L. B. G. Campanhol, S. A. O. da Silva, A. A. de Oliveira and V. D. Bacon, "Power Flow and Stability Analyses of a Multifunctional Distributed Generation System Integrating a Photovoltaic System With Unified Power Quality Conditioner," *IEEE Trans. Power Electron.*, vol. 34, no. 7, pp. 6241-6256, July 2019.
- [14] L. B. G. Campanhol, S. A. O. da Silva, A. A. de Oliveira and V. D. Bacon, "Dynamic Performance Improvement of a Grid-Tied PV System Using a Feed-Forward Control Loop Acting on the NPC Inverter Currents," *IEEE Trans. Ind. Electron.*, vol. 64, no. 3, pp. 2092-2101, March 2017.
- [15] R. K. Varma and E. M. Siavashi, "Enhancement of solar farm connectivity with smart PV inverter PV-STATCOM," *IEEE Trans. Sustain. Energy*, vol. 10, no. 3, pp. 1161-1171, July 2019.
- [16] S. K. Khadem, M. Basu and M. F. Conlon, "A review of parallel operation of active power filters in the distributed generation system," in *Proc. Eur. Conf. Power Electron. Appl.*, Birmingham, 2011, pp. 1-10.
- [17] S. J. Chiang and J. M. Chang, "Parallel operation of shunt active power filters with capacity limitation control," *IEEE Trans. Aerosp. Electron. Syst.*, vol. 37, no. 4, pp. 1312-1320, Oct. 2001.
- [18] S. Leng, I. Chung and D. A. Cartes, "Distributed operation of multiple shunt active power filters considering power quality improvement capacity," in *Proc. Int. Symp. Power Electron. Distrib. Gener. Syst.*, Hefei, 2010, pp. 543-548.
- [19] Y. Wang, Q. Xu and G. Chen, "Simplified multi-modular shunt active power filter system and its modelling," *IET Power Electron.*, vol. 8, no. 6, pp. 967-976, 6 2015.
- [20] Feng Ling et al., "Stability analysis of multiple Static Synchronous Compensators in parallel operation," in *Proc. IEEE Int. Power Electron. Motion Control Conf. (IPEMC-ECCE Asia)*, Hefei, 2016, pp. 1318-1322.
- [21] Y. Han, H. Li, P. Shen, E. A. A. Coelho and J. M. Guerrero, "Review of Active and Reactive Power Sharing Strategies in Hierarchical Controlled Microgrids," *IEEE Trans. Power Electron.*, vol. 32, no. 3, pp. 2427-2451, March 2017.
- [22] Y. Han, X. Ning, P. Yang and L. Xu, "Review of Power Sharing, Voltage Restoration and Stabilization Techniques in Hierarchical Controlled DC Microgrids," *IEEE Access*, vol. 7, pp. 149202-149223, 2019.
- [23] H. Mahmood, D. Michaelson and J. Jiang, "Reactive Power Sharing in Islanded Microgrids Using Adaptive Voltage Droop Control," *IEEE Trans. Smart Grid*, vol. 6, no. 6, pp. 3052-3060, Nov. 2015.
- [24] H. Zhang, S. Kim, Q. Sun and J. Zhou, "Distributed Adaptive Virtual Impedance Control for Accurate Reactive Power Sharing Based on Consensus Control in Microgrids," *IEEE Trans. Smart Grid*, vol. 8, no. 4, pp. 1749-1761, July 2017.
- [25] M. Yazdani and A. Mehrizi-Sani, "Distributed Control Techniques in Microgrids," *IEEE Trans. Smart Grid*, vol. 5, no. 6, pp. 2901-2909, Nov. 2014.
- [26] K. E. Antoniadou-Plytaria, I. N. Kouveliotis-Lysikatos, P. S. Georgilakis and N. D. Hatzargyriou, "Distributed and Decentralized Voltage Control of Smart Distribution Networks: Models, Methods, and Future Research," *IEEE Trans. Smart Grid*, vol. 8, no. 6, pp. 2999-3008, Nov. 2017.
- [27] Q. Wang, M. Cheng, Y. Jiang, W. Zuo and G. Buja, "A simple active and reactive power control for applications of single-phase electric springs," *IEEE Trans. Ind. Electron.*, vol. 65, no. 8, pp. 6291-6300, Aug. 2018.
- [28] D. Li and C. N. M. Ho, "A Delay-Tolerable Master-Slave Current-Sharing Control Scheme for Parallel-Operated Interfacing Inverters with Low-Bandwidth Communication," *IEEE Trans. Ind. Appl.*, vol. 56, no. 2, pp. 1575-1586, Mar.-Apr. 2020.